Wavelet analysis of EEG signals as a tool for the investigation of the time architecture of cognitive processes

R. Der[1]
Institut für Informatik, Univertsität Leipzig

U. Steinmetz[2]
Institut für Informatik, Univertsität Leipzig

April 28, 1997

[1]der@informatik.uni-leipzig.de
[2]steinmet@informatik.uni-leipzig.de

1 Introduction

Cognitive processes heavily rely on a dedicated spatio–temporal architecture of the underlying neural system — the brain. The spatial aspect is substantiated by the modularization as it has been brought to light in much detail by recent sophisticated neural imaging investigations. The time aspect is less well investigated although the role of time is prominent in several approaches to understanding the organization of the information processing in the brain. By way of example we mention (i) the synchronization hypothesis for the resolution of the binding problem, cf. [5] [4], [3] and the efforts to relate the information contained in observed spike rates back to the neuronal mechanisms underlying the cognitive event. In particular, in Refs. [1], [2] Amit et. al. tried to bridge the gap between the Miyashita data [10] and the hypothesis that associative memory is realized by the (strange) attractor states of dynamical systems.

These approaches are based on results from single cell recordings on mammals. For the human brain EEG analysis might play an analogous role. In fact EEG analysis can much contribute to the understanding of the spatio–temporal structure of the information processing in the brain. On the one hand exploiting the correlations between the EEG signals of different channels (sites) one may succeed in localizing the active modules in some cognitive event, cf. [9]. However as compared to the neural imaging techniques, the spatial resolution of this procedure is not very high. On the other hand, the time resolution of EEG is extremely good (typically 1 ms) and it is this high time resolution in combination with the spatial resolution which forms the special merit of EEG analysis.

However the above mentioned feature binding mechanism probably can not be observed in EEG since the neural assemblies synchronized are too small. One possible focus might be the oscillation hypothesis which relates the time architecture of cognitive processes back to the interplay of neuronal modules oscillating with different frequencies. Notably, Jensen and Lisman [8], [6], [7] developes detailes models for understanding the 7 ± 2 storage capacity of short term memory to the interplay of modules (neural networks) oscillating with frequencies in the θ and γ frequency bands.

The investigation of these effects requires a detailed time frequency analysis of the EEG signals. It is here where wavelets are at its best since they allow a most distinctive decomposition into frequency components while still keeping as much time information as possible. Hence in principle one may hope to directly observe stimulus induced oscillations of the neural assemblies involved in the cognitive event. In combination with the spatial resolution available this makes wavelet analysis of EEG signals a powerful vehicle of analyzing the spatio–temporal architecture of the brain.

The present paper tries to give an elementary introduction into the subject and to analyse some data in order to demonstrate the use of the method in practice. As a background, we introduce in Section 2 the Fourier and short time Fourier transforms in order to facilitate the comparison between different methods. A basic introduction to wavelet transforms may be found in Section 3. Pedagogical examples of WTs are presented in Section 4 and our wavelet

analysis of EEG signals is contained in Section 5. Details of the transforms, in particular the shape of time–frequency windows are relegated to the Appendices.

2 Fourier and Gabor transforms

Wavelets form a tool for the time–frequency analysis of complex signals. We will briefly introduce the Fourier and Gabor transforms in order to make the special merits of WTs explicite.

2.1 Fourier transforms and spectral density

Using (discrete) FTs one considers a given signal function $f(t)$ (inside an interval $t \in [0,T]$) as a superposition of frequency components given by harmonic functions

$$f(t) = \sum_{\omega} \alpha_\omega \sin\omega t + \beta_\omega \cos\omega t = \sum_{\omega} a_\omega \cos(\omega t + \phi_\omega) \quad \forall t \in [0,T] \tag{1}$$

the spectral density

$$S(\omega) = |\alpha_\omega|^2 + |\beta_w|^2 = |a_\omega|^2 \tag{2}$$

measuring the (square of the) amplitude of the component of frequency ω. For the continuous case we write correspondingly

$$f(t) = \frac{1}{\sqrt{2\pi}} \int_{-\infty}^{\infty} \mathrm{d}t e^{-i\omega t} \tilde{f}(\omega) \tag{3}$$

with the complex amplitude $\tilde{f}(\omega)$ and $S(w) = \left|\tilde{f}(\omega)\right|^2$. Note that any phase information is lost in the spectral density. Moreover, the FT analyses the global properties of the function only, i. e. any information on the time at which specific frequency components are active is not directly accessible in the FT.

2.2 Short–time Fourier and Gabor transforms

Short–time Fourier transforms (STFT) provide a time—frequency analysis of a signal $f(t)$ by using a time window which is moved over the signal, i. e. replace

$$f(t) \quad \rightarrow \quad f(t)\, G_\sigma(t - t_F) \tag{4}$$

and take the FT afterwards, the parameter σ denoting the width of the window and t_F its position on the time axis. A convenient window function was given by D. Gabor as

$$G_\sigma(\tau) = \frac{1}{\sqrt{2\pi}\sigma} e^{-\frac{\tau^2}{2\sigma^2}} \tag{5}$$

with the width of the window fixed by σ. The Fourier transform of the windowed function

$$f(t|t_F, \sigma) = f(t)\, G_\sigma(t - t_F)$$

is

$$\tilde{f}\left(\omega|t_F,\sigma\right)=\int_{-\infty}^{\infty}\mathrm{d}te^{-i\omega t}f\left(t|t_F,\sigma\right)=\int_{-\infty}^{\infty}\mathrm{d}te^{-i\omega t}f\left(t\right)G_\sigma\left(t-t_F\right) \tag{6}$$

which is also known as the Gabor transform of the function f

$$\tilde{f}\left(\omega|t_F,\sigma\right)=\left\{\mathcal{G}_\sigma^{t_F}f\left(t\right)\right\}_\omega \quad . \tag{7}$$

Using

$$\int_{-\infty}^{\infty}\mathrm{d}tG_\sigma\left(t\right)=1 \quad \forall\sigma \tag{8}$$

one has

$$\int_{-\infty}^{\infty}\mathrm{d}\tau\tilde{f}\left(\omega|\tau,\sigma\right)=\tilde{f}\left(\omega\right) \quad \forall\sigma$$

which may be viewed as the decomposition of the Fourier transform into Gabor transforms.

Alternatively we may also consider the Gabor transform as a window operation

$$\tilde{f}\left(\omega|t_F,\sigma\right)=\int_{-\infty}^{\infty}\mathrm{d}tW_\sigma\left(t-t_F\right)f\left(t\right) \tag{9}$$

where the window function is composed of the sin– and cos–Gabor functions

$$W_\sigma\left(\tau\right)=\frac{1}{\sqrt{2\pi}\sigma}e^{i\omega\tau}e^{-\frac{\tau^2}{2\sigma^2}}=\frac{1}{\sqrt{2\pi}\sigma}e^{-\frac{\tau^2}{2\sigma^2}}\left(\cos\omega t+i\sin\omega t\right) \tag{10}$$

and concentrated in

$$\left[t_F-\frac{\sigma}{\sqrt{2}},t_F+\frac{\sigma}{\sqrt{2}}\right]\times\left[\omega-\frac{1}{\sqrt{2}\sigma},\omega+\frac{1}{\sqrt{2}\sigma}\right] \tag{11}$$

which implies the well known uncertainty relation

$$\Delta t\Delta\omega=1/2 \tag{12}$$

The result (11) reveals the essential drawback of time–frequency analysis in terms of STFTs. The width of both the time and the frequency window is independent of the frequency once σ is chosen. Hence for given frequency component of $f\left(t\right)$ the number of the periods in the time window is proportional to the frequency analysed. However, independent of the frequency in order to define the frequency in a certain limit of accuracy one needs always only a certain number of periods. Hence actually the time–frequency window should adapt itself according to the frequency considered.

3 The wavelet transform

The essential advantage of the wavelet transform is the fact that the time-frequency window is flexible and does in fact adpat in such a way that there is always about the same number of periods of the frequency analysed in the time window.

3.1 Basic Wavelets

Wavelets are special window functions $\psi(t)$ with zero mean

$$\int_{-\infty}^{\infty} \mathrm{d}t \psi(t) = 0 \tag{13}$$

decaying sufficiently fast so that $\psi(t) \in L_2$, and $t\psi(t) \in L_2$. In frequency language this so called *admissibility condition* reads

$$\int_{-\infty}^{\infty} \mathrm{d}\omega \frac{\left|\tilde{\psi}(\omega)\right|^2}{|\omega|} < \infty \tag{14}$$

Examples are given by the Haar—function

$$\psi_H(t) = \begin{cases} 1 & \text{für} \quad 0 \leq x < \frac{1}{2} \\ -1 & \text{für} \quad \frac{1}{2} \leq x < 1 \\ 0 & \text{sonst} \end{cases} \tag{15}$$

and the above mentioned sin–Gabor function which we write here as

$$\psi(t) = \sin(2\pi\kappa_0 t)\, e^{-t^2/2} \tag{16}$$

where κ_0 is of the order of 1, see the Figures below.

3.2 The wavelet transform and time—frequency windows

The wavelet transformation is a window operation in the sense (9), the kernel (window) of the wavelet transform being obtained by translation and dilations of the chosen basis wavelets, i. e. we consider $\psi(t) \to \psi\left(\frac{t-b}{a}\right)$ and take this as the window function. Hence the **wavelet transform** is

$$f[b,a] = \{W_\psi f\}_{(b,a)} = \frac{1}{\sqrt{|a|}} \int_{-\infty}^{\infty} dt\, f(t)\, \psi^*\left(\frac{t-b}{a}\right) \tag{17}$$

From Appendix B (7.2) we find the time–frequency window as

$$[b - a\Delta_\psi, b + a\Delta_\psi,] \times \left[\frac{\omega_\psi}{a} - \frac{1}{a}\Delta_{\tilde{\psi}}, \frac{\omega_\psi}{a} + \frac{1}{a}\Delta_{\tilde{\psi}}\right] \tag{18}$$

Now $1/a = v$ can obviously be interpreted as a frequency, i. e. $\omega_F = \frac{\omega_\psi}{a} = v\omega_\psi$ is the center of the frequency window in units of the center frequency ω_ψ of the basic wavelet. This one is roughly given by κ_0 in the special case (16) of the sin–Gabor wavelet used throughout the present paper. The area of the time window is obviously independent of a. However, its form changes as a function of frequency $v = \frac{1}{a}$ in such a way that the **relative** error in frequency is kept constant for all frequencies.

3.3 Inverse transformation

For the sake of completeness we give the formula for the reconstruction of the signal from the wavelet transform (inverse transformation). Let

$$\widehat{f}\,(b,a) := \{W_\psi f\}\,(b,a)$$

be the wavelet transform of a function $f\,(t)$ with basis wavelet $\psi\,(t)$. Then

$$f\,(t) = \frac{1}{C_\psi}\int_{-\infty}^{\infty}\int_{-\infty}^{\infty} \mathrm{d}a\,\mathrm{d}b\,\widehat{f}\,(b,a)\,\frac{1}{a^2\sqrt{|a|}}\psi\left(\frac{t-b}{a}\right) \tag{19}$$

where

$$C_\psi = \int_{-\infty}^{\infty} d\omega \frac{\left|\tilde{\psi}\,(\omega)\right|^2}{|\omega|} \tag{20}$$

cf. (14).

4 Pedagogical Examples of Wavelet Transforms

Let us consider some relevant examples of wavelets $\psi\left(\frac{t-b}{a}\right)$ with the basic wavelets

$$\psi\,(t) = \sin\left(2\pi\kappa_0 t\right)\exp\left(-\frac{t^2}{2}\right) \tag{21}$$

(the sin–Gabor–wavelet introduced above) which we use everywhere in the present paper.

Now, let us consider first the time localized superposition of four harmonics:

$$f\,(t) = \sum_{i=1}^{4} \sin 2\pi v_i(t-0.7)\,e^{-\frac{1}{2}\left(\frac{t-0.7}{0.1}\right)^2} \tag{22}$$

depicted in Fig. 1. Its wavelet transform for $\kappa_0 = 0.5$ is shown in Fig. 2 Throughout the paper we always depict the square of the wavelet transform and use a twice iterated gray scale for coding these values, the gray background corresponding to the zero level. We observe in Fig. 2 an extreme time resolution since $\kappa_0 = 0.5$ means that the width of the time window is just that of a single oscillation at the frequency considered. Nevertheless the frequency resolution is sufficient so that one still can discriminate the different frequencies contained in the signal. The following picture Fig. 3 is obtained with the basic wavelet with $\kappa_0 = 2$ so that there are about four to five periods of oscillations which form the basis of the analysis of the signal. Hence the frequency resolution is much improved which of course has to be paid by a loss in time resolution. This is seen best by the wings in the low frequency regime caused by the widening with decreasing frequency of the time window.

The following example is that of a twin bump

$$f\,(t) = e^{-\frac{1}{2}\left(\frac{t-0.5}{0.1}\right)^2} - e^{-\frac{1}{2}\left(\frac{t-0.7}{0.2}\right)^2} \tag{23}$$

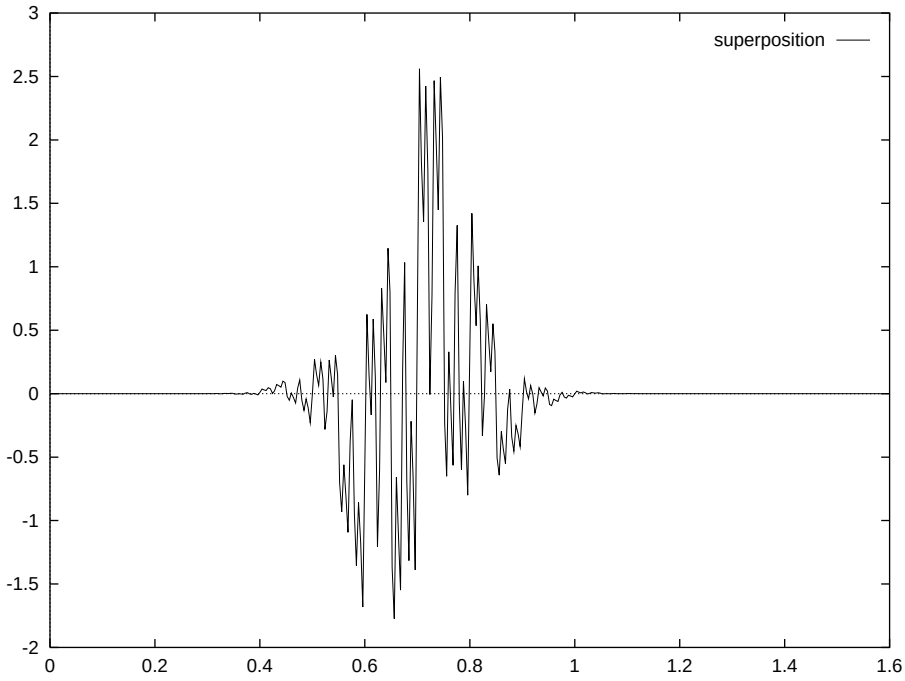

Figure 1: The function $f(t) = \sum_{i=1}^{4} \sin 2\pi v_i (t - 0.7)\, e^{-\frac{1}{2}\left(\frac{t-0.7}{0.1}\right)^2}$ with $v_1 = 3$, $v_2 = 10$, $v_3 = 30$, $v_4 = 70\,\mathrm{Hz}$.

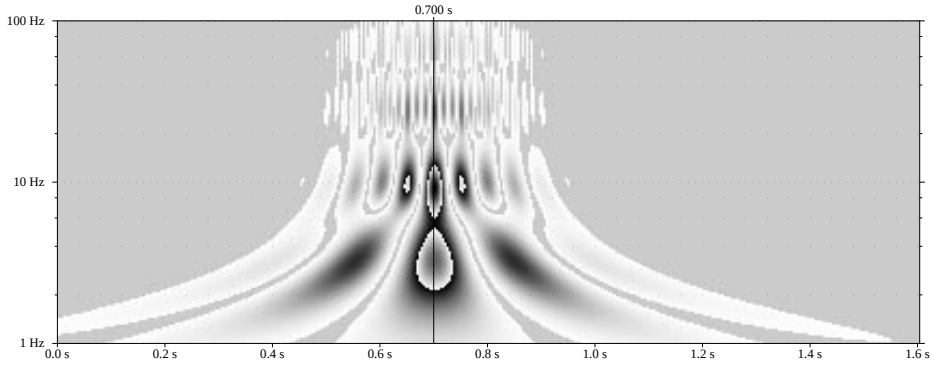

Figure 2: Wavelet transform with $\kappa_0 = 0.5$ of the function $f(t) = \sum_{i=1}^{4} \sin 2\pi v_i (t - 0.7)\, e^{-\frac{1}{2}\left(\frac{t-0.7}{0.1}\right)^2}$ with $v_1 = 3, v_2 = 10, v_3 = 30$ and $v_4 = 70\,\mathrm{Hz}$. The transformation is according to the standard expression, i. e. there is no extra scaling factor in order to enhance high frequency components.

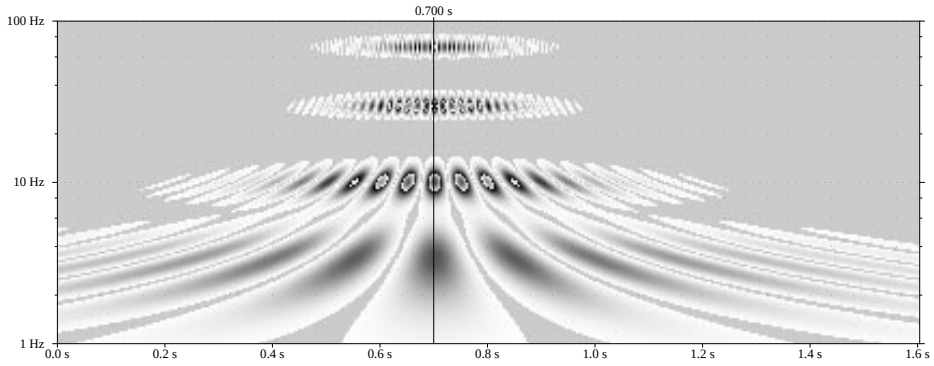

Figure 3: Wavelet transform with $\kappa_0 = 2$ of the function $f(t) = \sum_{i=1}^{4} \sin 2\pi v_i (t - 0.7)\, e^{-\frac{1}{2}\left(\frac{t-0.7}{0.1}\right)^2}$ with $v_1 = 3, v_2 = 10, v_3 = 30$ and $v_4 = 70\,\mathrm{Hz}$. The transformation is according to the standard expression, i. e. there is no extra scaling factor in order to enhance high frequency components.

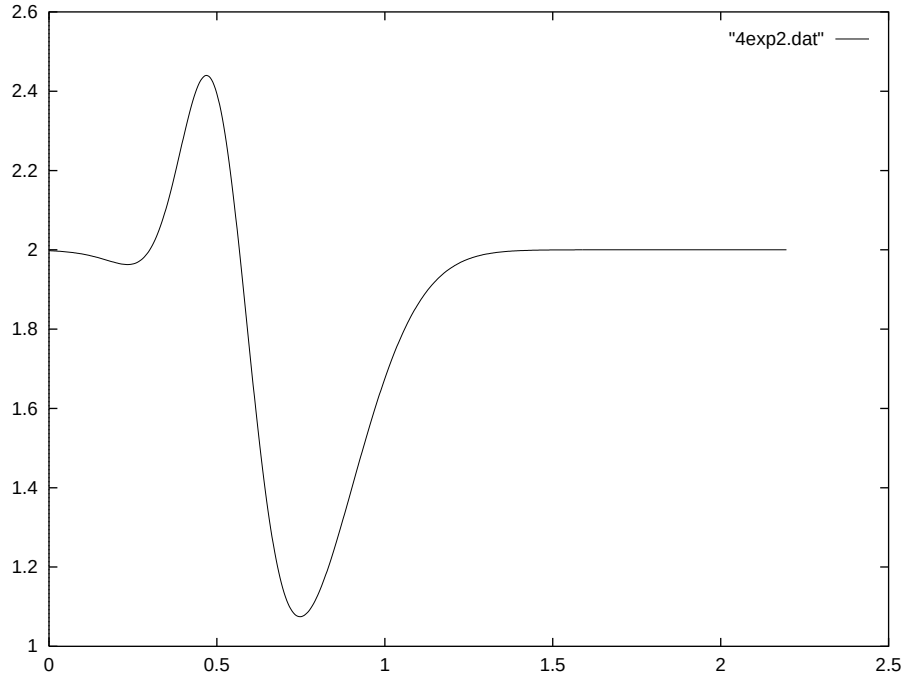

Figure 4: The function $f(t) = e^{-\frac{1}{2}\left(\frac{t-0.5}{0.1}\right)^2} - e^{-\frac{1}{2}\left(\frac{t-0.7}{0.2}\right)^2} + 2$ mimicing the average EEG response to novel events.

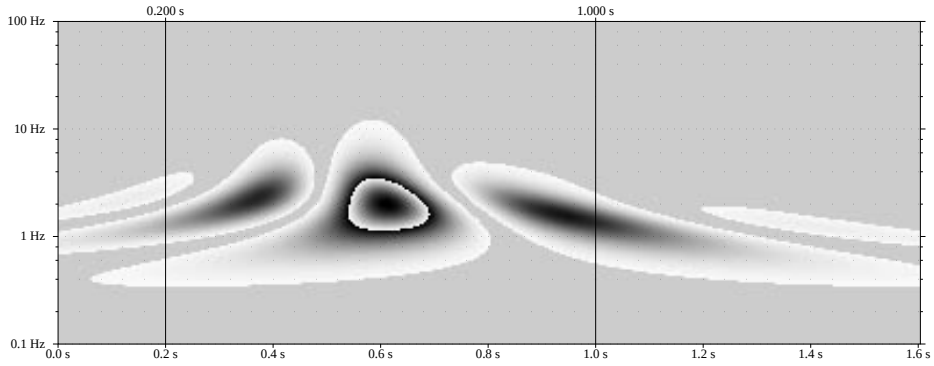

Figure 5: Wavelet transform of the function $f(t) = e^{-\frac{1}{2}\left(\frac{t-0.5}{0.1}\right)^2} - e^{-\frac{1}{2}\left(\frac{t-0.7}{0.2}\right)^2}$.

depicted in Fig. 4 which is to mimic the average EEG response to novel events.

Its wavelet transform obtained from the standard expression (17) is multiplied with an additional amplitude correction factor $v^2 = 1/a^2$ in order to enhance high frequencies in the same way as this is done with the EEG signals shown below. The point of studying the function (23) is the behaviour of the WT at high frequencies, i. e. the question as to wether there are higher order harmonics of substantial amplitude. The pictures clearly demonstrate that this is not the case. We may conclude from this crude argument that the components of higher frequency (above 10 Hz say) observed in the EEG signals are not caused by the P100 or P300 components itself but are genuine signals of neuronal modules oscillating at these frequencies.

As a finale example we study the role of interference effects if the signal contains different frequencies which are so close in frequency that the wavelet can not resolve the frequencies so that two or several frequencies contribute to the transform. Then, the value of the transform at given a, b depends on the phase relation of the components contributing.

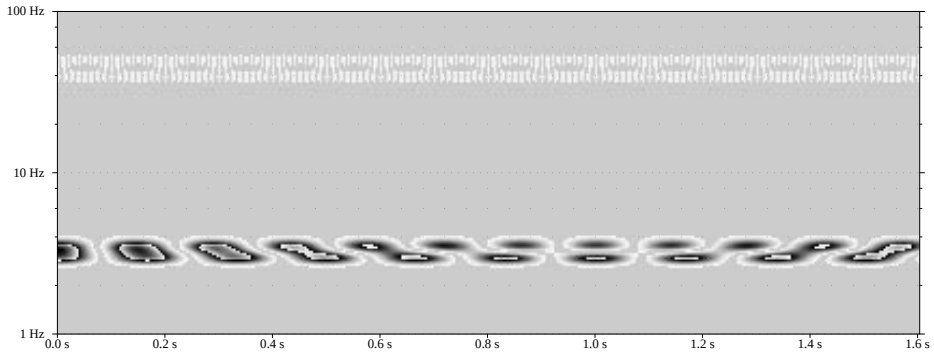

Figure 6: Interferencies occurring in the wavelet trasforms of a signal function $f(t)$ consisting of two frequency bands of closely related frequencies.

5 Wavelet analysis of EEG signals

We study in the following EEG recordings obtained from human subjects at 112 electrodes. Stimuli have been target and standard tones of 2000 and 1000 Hz and a collection of so called novels comprised of various noises. The stimuli of duration of 100 ms have been presented at regular intervals of 800 ms. The task consisted in counting the target events. We first depict in Fig. 7 the recordings at one of the electrodes over a period of time comprising 4 events. The WT

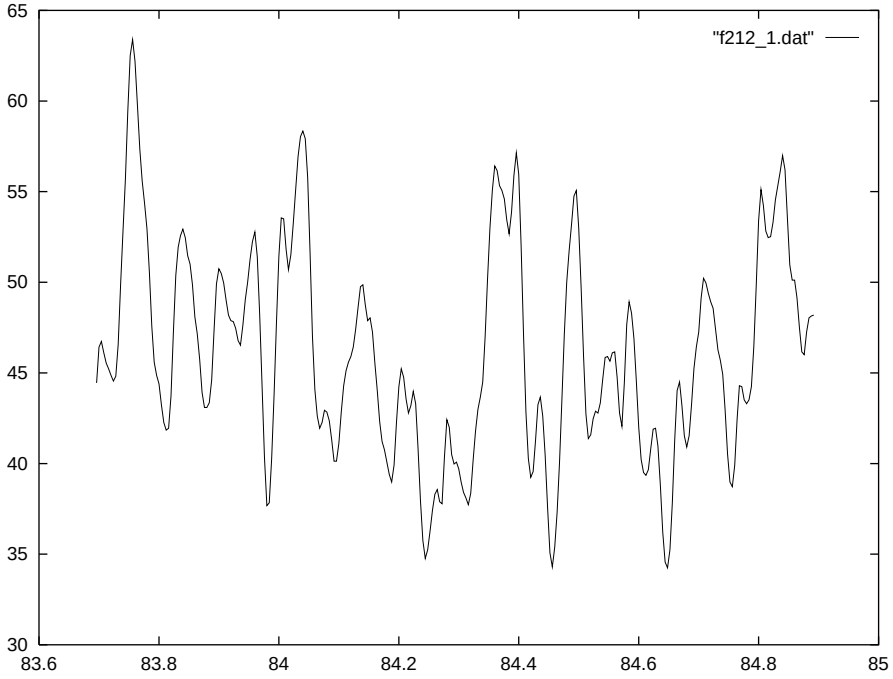

Figure 7: The voltage recorced at a selected electrode over time

for $\kappa_0 = 0.5$ and $\kappa_0 = 2$ may be found on the following pages. We depicted the WTs in the same way as in Sec. 4 above, i. e. we depict the square of the WT multiplied by a correction factor of $v^2 = 1/a^2$ introduced in order to better display the behaviour at high frequencies. We show the WTs first in a 3-d representation in Figs. 8 and 9. Afterwards we use as before the twice iterated gray scale for coding these values, the gray background corresponding to the zero level. The WTs are normalized with a normalization factor common to the whole time interval.

We clearly see that besides the activities at low frequencies which are related to the systematic response from the dipoles found in [9], we also observe systematic belts of more or less constant frequency at higher frequencies. These might be related to the neural oscillations mentioned in the introduction. One way to find out about the relations of these oscillations to the events consists in studying the phase of the oscillations relative to the events. For this purpose we investigated the average of the WTs over time. We studied both the average of the WT itself as well as the average of the square of the WTs. Now as is clearly seen from the WTs of single events like that shown in Figs. 10

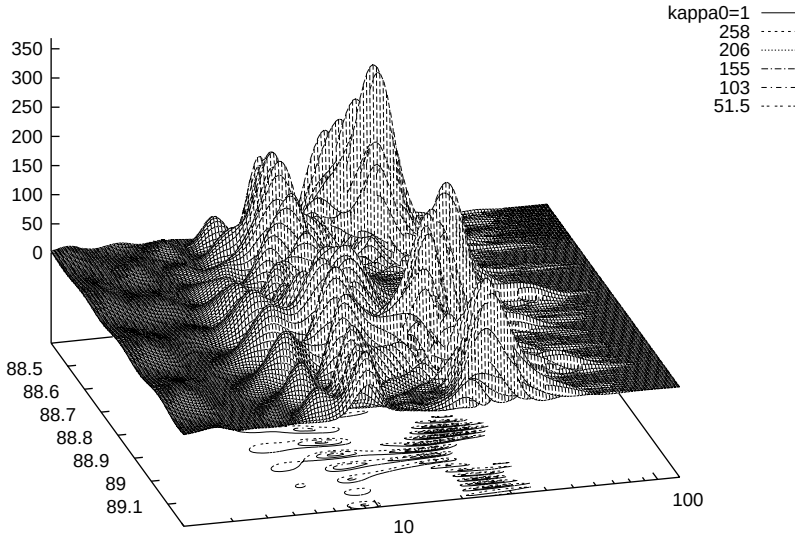

Figure 8: Wavelet transforms with $\kappa_0 = 1$ of the EEG signals of Fig. 7

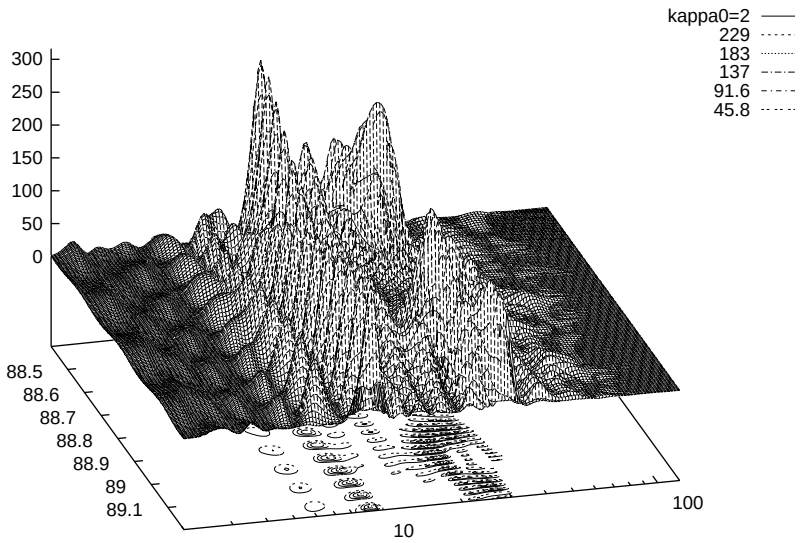

Figure 9: Wavelet transforms $\kappa_0 = 2$ of the EEG signals of Fig. 7

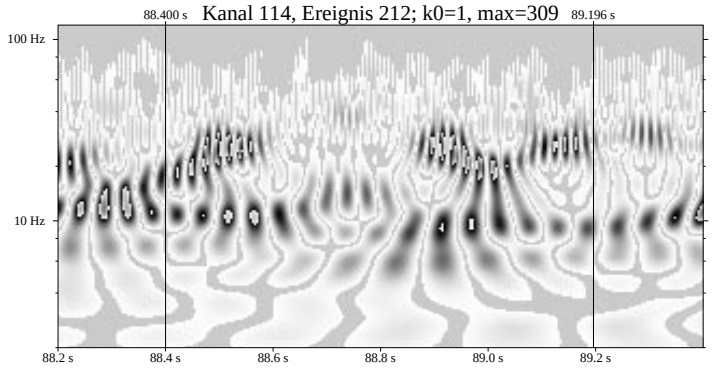

Figure 10: Greyscale image of the Wavelet transforms with $\kappa_0 = 1$ of the EEG signals of Fig. 7

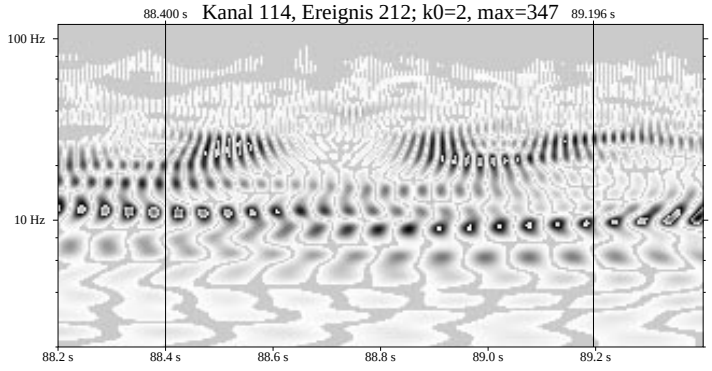

Figure 11: Greyscale image of the Wavelet transforms $\kappa_0 = 2$ of the EEG signals of Fig. 7

and 11 oscillations do last over a certain period of time only. Hence if there is no relation to the stimulus the phase of each of the oscillatory epochs will be uncorrelated with the onset of the stimulation. In other words, the phase of a definite oscillation is randomly distributed over the events. Hence upon averaging any definite structure related to the phase should average out. This cleary seen in the Figs. 12 through 17 (see the following pages) to happen for most of the active frequencies. However for the frequency band at about 17 Hz we observe the opposite behaviour. Here we see a detailed structure which can only be explained by the assumption that the oscillation becomes phase locked by the stimulus.

In order to exclude statistical effects (the structure might stem from one single event which majorises in the average all the others) we depict in Fig. 18

the partial averages obtained from setting a threshold and including into the averaging only events with amplitude (in the frequency band considered =17 Hz) of the WT below the threshold. Fig. 18 clearly shows that (i) the phase locking is valid for all oscillations of arbitrary amplitude and that (ii) the observed structure is not a statistical effect since it is valid both in the total and in all the partial averages.

Of the several points of interest connected with this oscillatory behaviour we note that from the pictures it might seem that the oscillation is composed of two components of slightly different frequency and that the frequency of the two components is not very stable, i. e. we have a nonlinear effect of frequency shift due to the coupling to other oscillators. It would be interesting to find out whether we observe here a case of **entrainment** of the oscillations by the stimulus.

From scrutinizing the transforms over all the channels we also observe a second phase locking frequency at 10 Hz with the interesting property to become strong towards the end of the ISI.

6 Conclusions

In the present paper we presented the wavelet transforms as a method for studying the time architecture of cognitive processes. Of course, time–frequency analysis of EEG signals is not a new subject. Even more, all results available from wavelet analysis can also be obtained from using filter banks of conveniently tuned filters, e. g. However what we hoped to demonstrate is the fact that by using a convenient representation of the WTs one can hope to find new effects in the time architecture of cognitive processes by visual scrutinization of the wavelet diagrams.

In particular, considering the hypothesis that time architeture of perception is based on the interplay of oscillatory networks oscillating with very different frequencies, wavelet transforms in a convenient representation might be helpful in discovering these structures in the EEG recordings with specific psychophysical experiments. The phase locking by the stimulus of the 10 and 17 Hz oscillations found in the present paper might be a first hint in this direction. We hope in the near future to find the localizations of the corresponding neural

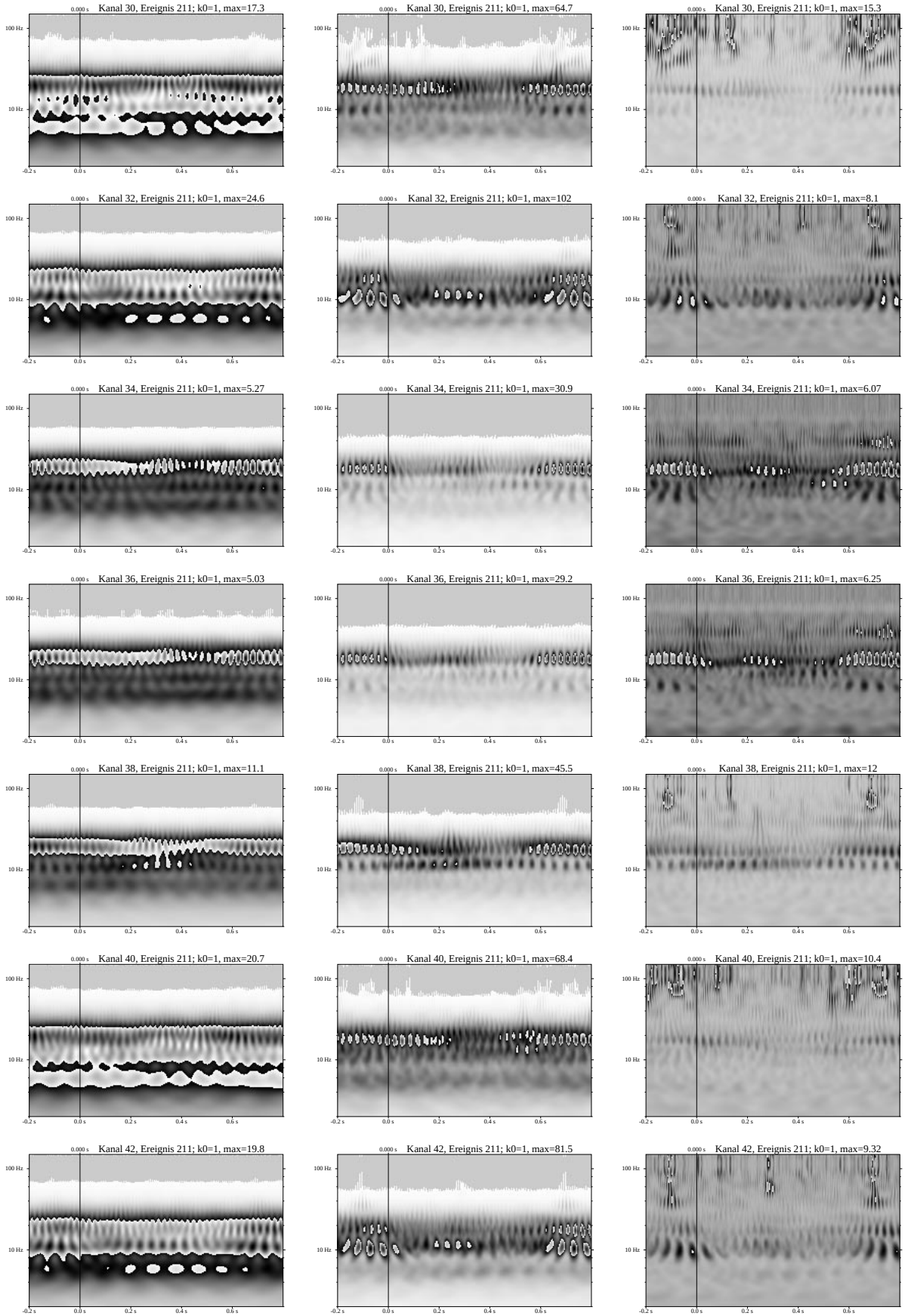

Figure 12: left: Averages of the square of the WTs over the events for $\kappa_0 = 1$ and event type 211 (standards). The dispersion is shown in the middle and the relative dispersion is shown in the right column.

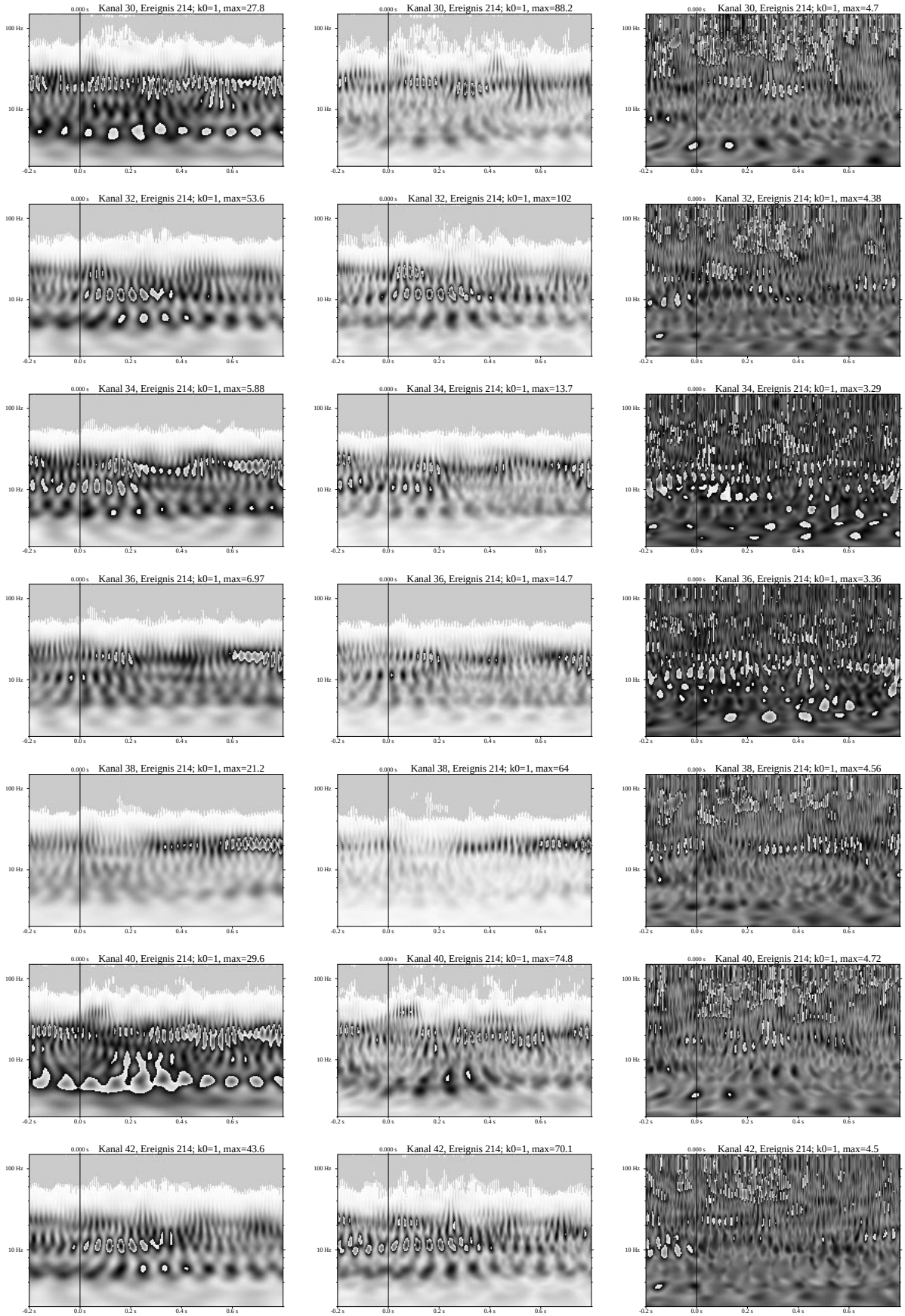

Figure 13: Averages of the square of the WTs over the events for $\kappa_0 = 1$ and event type 214 (novels).

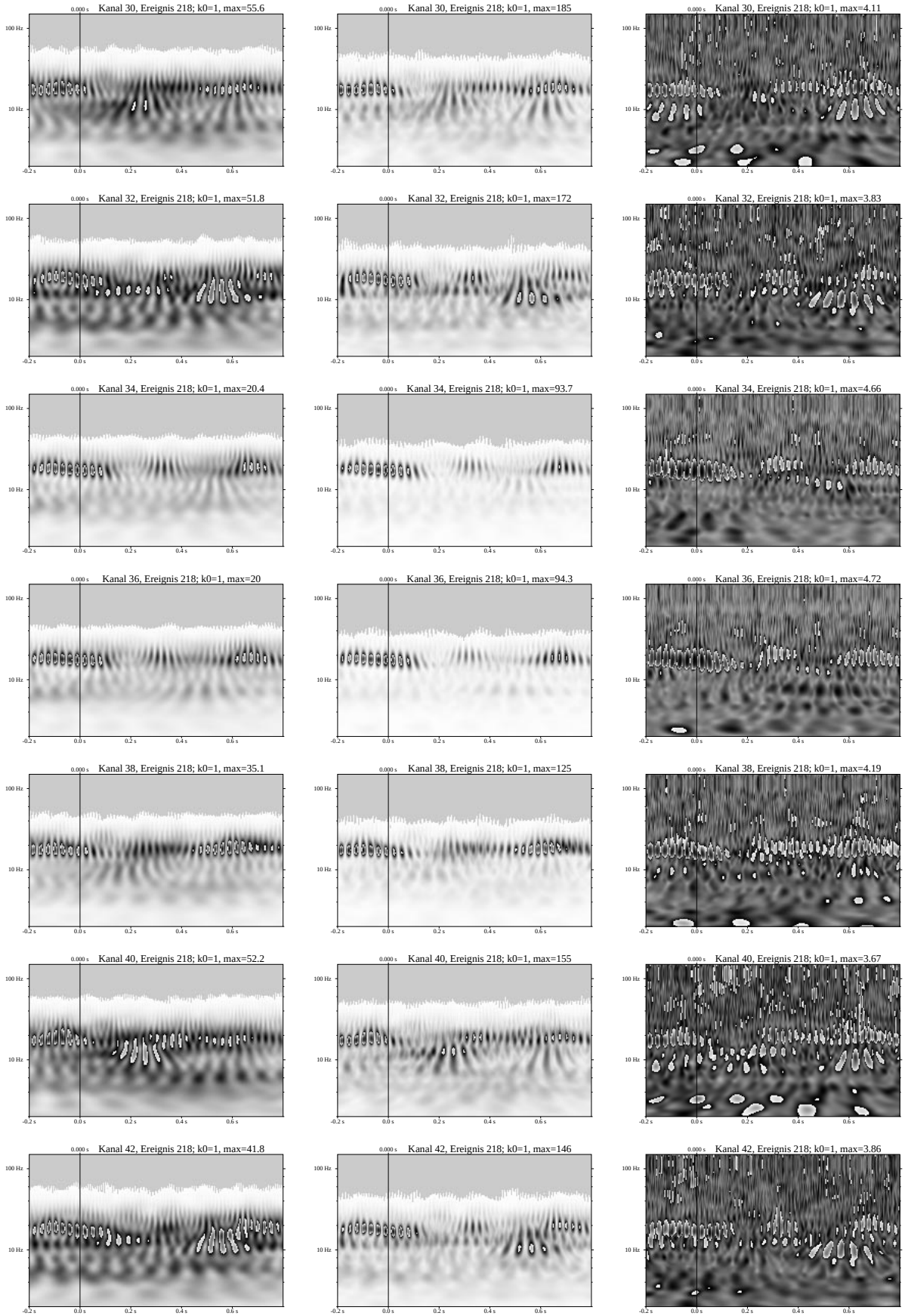

Figure 14: Averages of the square of the WTs over the events for $\kappa_0 = 1$ and event type 218 (novels).

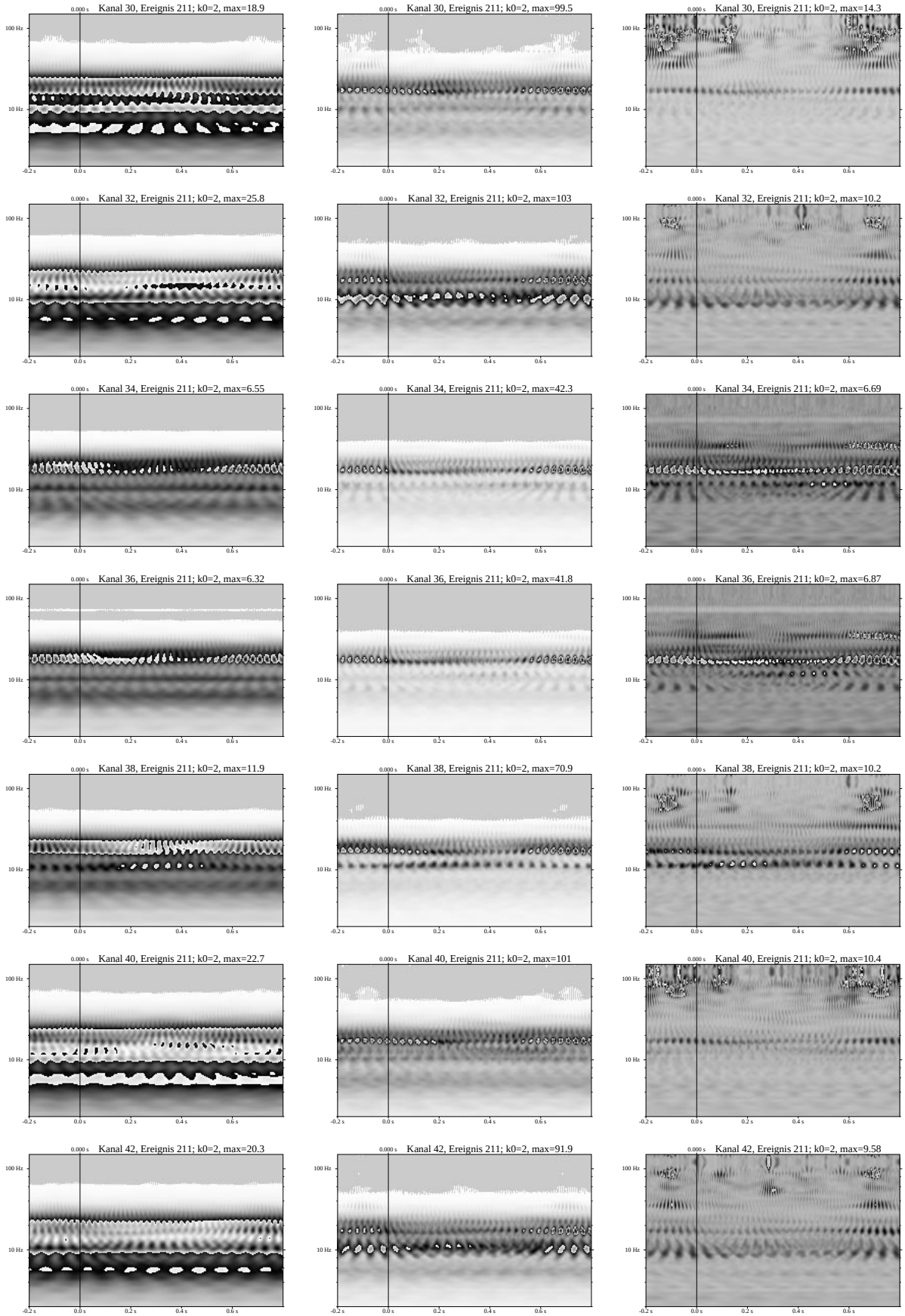

Figure 15: Averages of the square of the WTs over the events for $\kappa_0 = 2$ and event type 211 (standard).

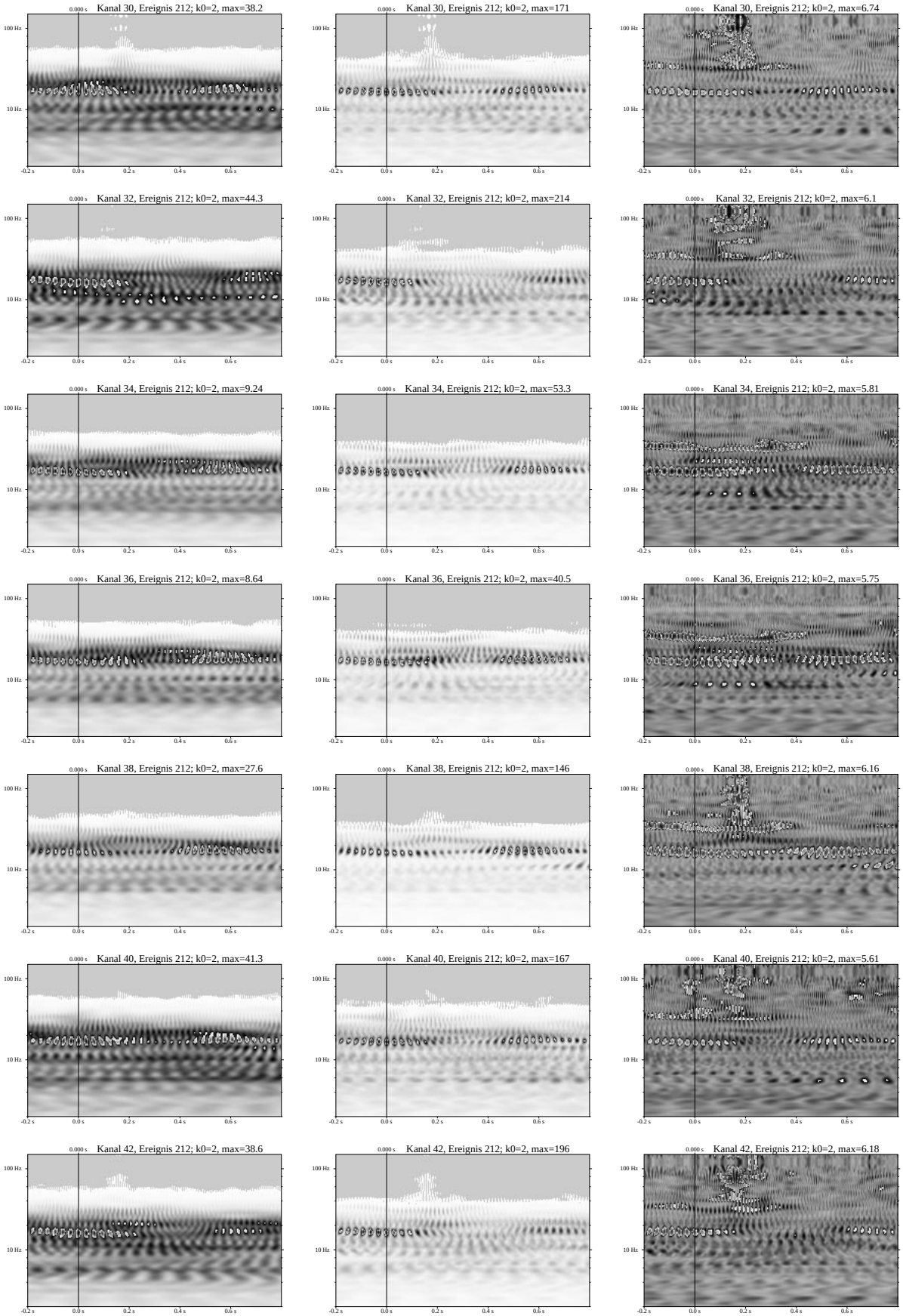

Figure 16: Averages of the square of the WTs over the events for $\kappa_0 = 2$ and event type 212 (target).

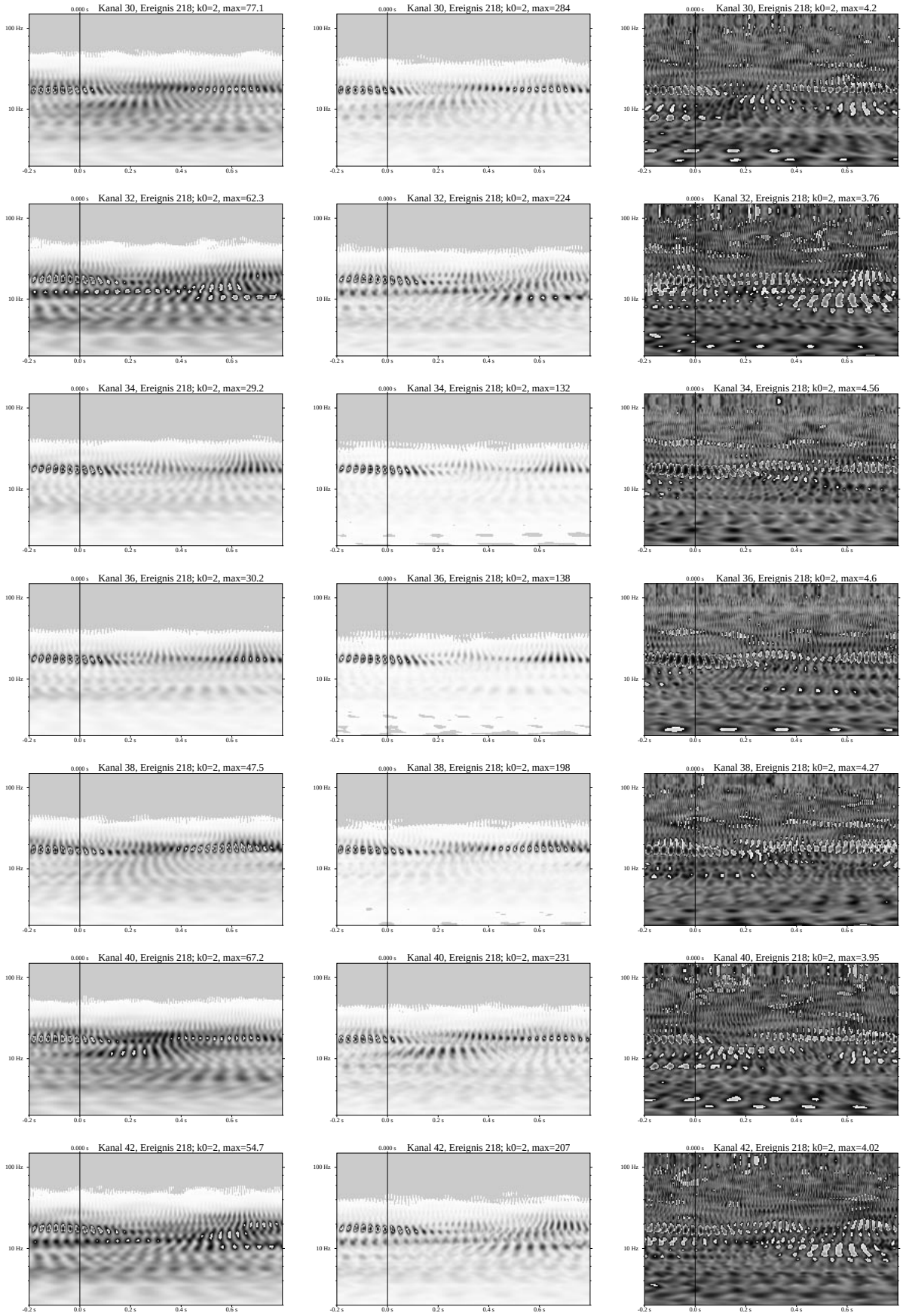

Figure 17: Averages of the square of the WTs over the events for $\kappa_0 = 2$ and event type 218 (novels)

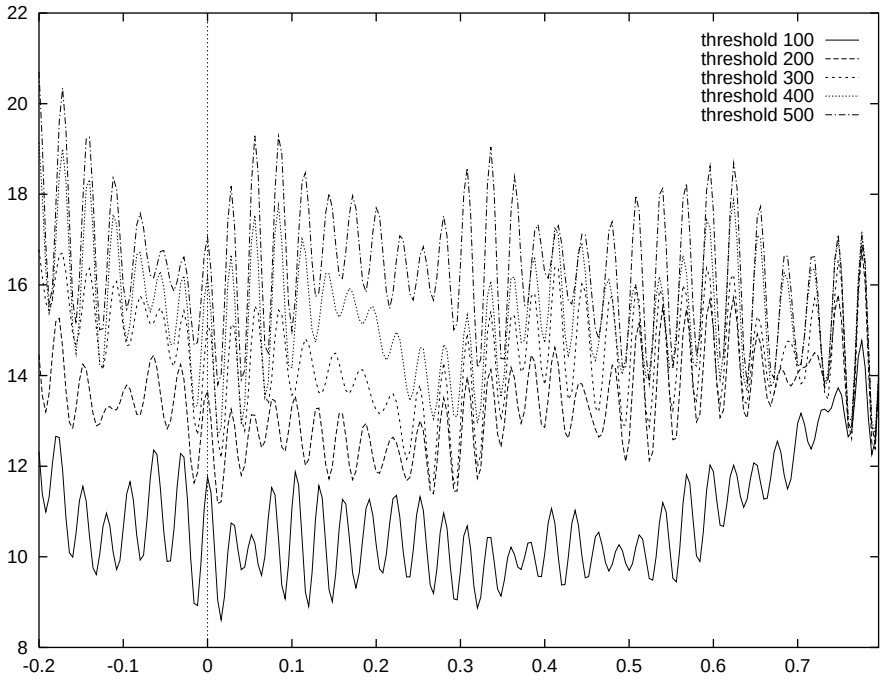

Figure 18: Partial averages of the squares of the WT over events including but the events with strength of the pertinent 17 Hz oscillations below a threshold.

oscillators in order to learn more about their role in the information processing and in particular about their interplay with the dipoles identified as the sources of the N100 and P300 responses.

7 Appendices

7.1 Appendix A: Time–frequency windows for STFTs

Alternatively we may also consider consider the Gabor transform as a window operation according to (9)

$$\tilde{f}\left(\omega|t_F,\sigma\right)=\int_{-\infty}^{\infty}\mathrm{d}tW_\sigma\left(t-t_F\right)f\left(t\right) \tag{24}$$

There is an important relation between the windows in the time and in the frequency domain. Let us consider the set of all functions $f\left(t\right)\in L_2$ and propose that there is a corresponding window function $H\left(\omega\right)$ in frequency space so that

$$\int_{-\infty}^{\infty}\mathrm{d}tf\left(t\right)G_{(\sigma,\omega)}^{t_F}\left(t\right)=\int_{-\infty}^{\infty}\mathrm{d}\eta\,\tilde{f}\left(\eta\right)H^*\left(\eta\right)\qquad\forall f\in L_2 \tag{25}$$

Using Parsevals identity one easily finds that $H\left(\omega\right)$ is essentially the Fourier transform of the time window function. Hence for the special case of the Gabor function one has

$$\begin{aligned}H\left(\eta\right) &= \widetilde{G_{(\sigma,\omega)}^{t_F}}\left(\eta\right)=\int_{-\infty}^{\infty}\mathrm{d}te^{-i\eta t}G_{(\sigma,\omega)}^{t_F}\left(t\right)\\ &= e^{-it_F(\eta-\omega)}e^{-\sigma^2(\eta-\omega)^2/2}\end{aligned} \tag{26}$$

so that the window functions in time and frequency space are of the same functional form differing only in width

$$\frac{1}{\sqrt{2\pi}\sigma}e^{i\omega(t-t_F)}e^{-\frac{(t-t_F)^2}{2\sigma^2}}\quad\Leftrightarrow\quad\frac{1}{2\pi}e^{-it_F(\eta-\omega)}e^{-\sigma^2(\eta-\omega)^2/2} \tag{27}$$

The root mean square width Δt in time is found as $\sigma/\sqrt{2}$ the corresponding width $\Delta\omega$ in frequency is $1/\sqrt{2}\sigma$. Hence times t and frequencies η which essentially are represented by the transform are from the time–frequency window

$$\left[t_F-\frac{\sigma}{\sqrt{2}},t_F+\frac{\sigma}{\sqrt{2}}\right]\times\left[\omega-\frac{1}{\sqrt{2}\sigma},\omega+\frac{1}{\sqrt{2}\sigma}\right] \tag{28}$$

corresponding to the uncertainty relation

$$\Delta t\Delta\omega=1/2 \tag{29}$$

independent of the frequency.

7.2 Appendix B: Time–frequency windows for wavelet transforms

Introducing the position t_ψ

$$t_\psi=\frac{1}{\left\|\psi\right\|^2}\int_{-\infty}^{\infty}\mathrm{d}t\,t\,\left|\psi\left(t\right)\right|^2$$

and root mean square width $2\Delta_\psi$,

$$\Delta_\psi = \frac{1}{\|\psi\|}\sqrt{\int_{-\infty}^{\infty} \mathrm{d}t\ (t-t_\psi)^2\ |\psi(t)|^2}$$

of the basis wavelet we find that the tranlation and dilation operation transform

$$t_\psi \to t_F = at_\psi + b, \qquad \Delta_\psi \to \Delta_F = a\Delta_\psi \tag{30}$$

The signal is consequently localized in the time window

$$[b + at_\psi - a\Delta_\psi, b + at_\psi + a\Delta_\psi,] = [t_F - \Delta_F, t_F + \Delta_F]$$

On the other hand we find for the frequency window (in the same way as with the Gabor transforms) the frequency window as

$$\left[\frac{\omega_\psi}{a} - \frac{1}{a}\Delta_{\tilde{\psi}}, \frac{\omega_\psi}{a} + \frac{1}{a}\Delta_{\tilde{\psi}}\right]$$

where ω_ψ is the center frequency

$$\omega_\psi = \frac{1}{\left|\left|\tilde{\psi}\right|\right|^2}\int_{-\infty}^{\infty} \mathrm{d}\omega\omega \left|\tilde{\psi}(\omega)\right|^2$$

and $2\Delta_{\tilde{\psi}}$ the root mean square width of the basis wavelet in the frequency space. Hence the time–frequency window is

$$[b + at_\psi - a\Delta_\psi, b + at_\psi + a\Delta_\psi,] \times \left[\frac{\omega_\psi}{a} - \frac{1}{a}\Delta_{\tilde{\psi}}, \frac{\omega_\psi}{a} + \frac{1}{a}\Delta_{\tilde{\psi}}\right] \tag{31}$$

or

$$[t_F - \Delta_F, t_F + \Delta_F] \times \left[\omega_F - \tilde{\Delta_F}, \omega_F + \tilde{\Delta_F}\right]$$

The area of the time window is obviously independent of a. However, its form changes as a function of a in such a way that the time extension is inverse proportional to the center frequency ω_F. as it should be. This special property is also reflected by the fact that the ratio between center frequency ω_F and band width $\Delta_{\tilde{F}} = \frac{2}{a}\Delta_{\tilde{\psi}}$ of the frequency window is independent of ω_F itself

$$\frac{\omega_F}{\Delta_{\tilde{F}}} = Q = \frac{\omega_\psi}{\Delta_{\tilde{\psi}}} \tag{32}$$

This is called constant Q filtering in signal processing.

Remarks:

- The function $\frac{1}{\sqrt{|a|}}\psi\left(\frac{t-b}{a}\right)$ is used for transformation in both directions in the same way as $e^{i\omega t}$ in the FT (consider $e^{-i\omega t} = \left(e^{i\omega t}\right)^*$).

1. For the time frequency analysis the frequencies ω_F are always poitive. The basis wavelets then have to abey the admissibility condition

$$\int_0^\infty \mathrm{d}\omega \frac{\left|\tilde{\psi}\left(\omega\right)\right|^2}{\omega} = \frac{1}{2} C_\psi < \infty \tag{33}$$

The corresponding reconstruction formula is

$$f\left(t\right) = \frac{2}{C_\psi} \int_0^\infty \mathrm{d}a \frac{1}{a^2} \left[\int_{-\infty}^\infty \mathrm{d}b\, \widehat{f}\left(b,a\right) \frac{1}{\sqrt{a}} \psi\left(\frac{t-b}{a}\right) \right] \tag{34}$$

which differs only by a factor of 2 from 19.

References

[1] D. J. Amit and N. Brunel. Global spontaneous activity and local structured (learned) delay activity in cortex. *Cerebral Cortex*, 7, 1996.

[2] D. J. Amit, S. Fusi, and V. Yakovlev. Working memory (attractor cell) in it cortex. *Neural Computation*, 1997.

[3] A. K. Engel, P. König, and W. Singer. Direct physiological evidence for scene segmentation by temporal coding. *Proc. Natl. Acad. Sci. USA*, 88:9136–9140, 10 1991.

[4] C. M. Gray, P. König, A. K. Engel, and W. Singer. Oscillatory responses in cat visual cortex exhibit inter-columnar synchronization which reflects global stimulus properties. *Nature*, 338:334–337, 1989.

[5] C. M. Gray and W. Singer. Stimulus-specific neuronal oscillations in orientation columns of cat visual cortex. *Proceedings of the National Academy of Sciences, USA*, 86:1698–1702, 1989.

[6] O. Jensen, M. A. P. Idiart, and J. Lisman. Physiologically realistic formation of autoassociative memory in networks with theta/gamma oscillations: Role of fast NMDA channels. *Learning and memory*, 3:243 – 256, 1996.

[7] O. Jensen and J. E. Lisman. Hippocampal ca3 region predicts memory sequences: Accounting for the phase precession of place cells. *Learning and Memory*, 3:279 – 287, 1996.

[8] O. Jensen and J. E. Lisman. Novel lists of 7+/-2 known items can be stored reliably in an oscillatory short term memory network: Interaction with long term memory. *Learning and Memory*, 3:257 – 236, 1996.

[9] A. Mecklinger and P. Ullsperger. The p300 novel and target events: A spatio–temporal dipole model analysis. *Cognitive Neurosciences and Neuropsychology*, 7:241 – 245, 1995.

[10] Y. Miyashita. Neuronal correlate of visual associative long-term memory in the primate temporal cortex. *Nature*, 335:817–820, 10 1988.

[11] R. F. Port and T. V. Gelder. *Mind as motion: Explorations in the dynamics of cognition.* Massachusetts Institute of Technology, 1995.